gradient, $d\phi/dz$, across the condensate. Such a gradient may be imprinted by a condensate velocity, because $d\phi/dz = mv/\hbar$, where $m$ is the atomic mass. If $N_s$ is identified with $\phi/\pi$, the model predicts $N_s \propto v$, in agreement with the observed $v$-dependent part of $N_s$. Furthermore, for the largest $v$ and for parameters consistent with the experiment, the model gives $N_s \approx 15$, in rough agreement with observation.

For a soliton with $a = -3a_o$, the calculated maximum number of atoms that ensures stability is only ~6,000 per soliton[11,13], which accounts for far fewer atoms than the number contained in the initial repulsive condensate. Apparently, most of the atoms from the collapsing condensate are lost, while only a small fraction remain as solitons. Immediately after switching $a$ from positive to negative, we observe a diffuse background of atoms spreading out axially. This observation is reminiscent of the jet emitted by a $^{85}$Rb condensate after switching from repulsive to attractive interactions[5]. In our system, which is in the quasi-1D regime, the remnant atoms form solitons with atom number near their stability limit.

The remarkable similarities between bright matter-wave solitons and optical solitons in fibres[26] emphasize the intimate connection between atom optics with Bose–Einstein condensates[27] and light optics. Many issues remain to be addressed, however, including the dynamical process of soliton formation. In addition, further investigation of soliton interactions and collisions could be undertaken with this system. Finally, we speculate that an 'atomic soliton laser', based on bright matter-wave solitons, may prove useful for precision measurement applications, such as atom interferometry[28]. □

Received 19 March; accepted 18 April 2002.
Published online 1 May 2002, DOI 10.1038/nature747.

1. Ruprecht, P. A., Holland, M. J., Burnett, K. & Edwards, M. Time-dependent solution of the nonlinear Schrodinger equation for Bose-condensed trapped neutral atoms. *Phys. Rev. A* **51,** 4704–4711 (1995).
2. Bradley, C. C., Sackett, C. A. & Hulet, R. G. Bose-Einstein condensation of lithium: observation of limited condensate number. *Phys. Rev. Lett.* **78,** 985–989 (1997).
3. Sackett, C. A., Gerton, J. M., Welling, M. & Hulet, R. G. Measurements of collective collapse in a Bose-Einstein condensate with attractive interactions. *Phys. Rev. Lett.* **82,** 876–879 (1999).
4. Gerton, J. M., Strekalov, D., Prodan, I. & Hulet, R. G. Direct observation of growth and collapse of a Bose–Einstein condensate with attractive interactions. *Nature* **408,** 692–695 (2000).
5. Donley, E. A. *et al.* Dynamics of collapsing and exploding Bose–Einstein condensates. *Nature* **412,** 295–299 (2001).
6. Stegeman, G. I. & Segev, M. Optical spatial solitons and their interactions: Universality and diversity. *Science* **286,** 1518–1523 (1999).
7. Dalfovo, F., Giorgini, S., Pitaevskii, L. P. & Stringari, S. Theory of Bose-Einstein condensation in trapped gases. *Rev. Mod. Phys.* **71,** 463–512 (1999).
8. Burger, S., Bongs, K., Dettmer, S., Ertmer, W. & Sengstock, K. Dark solitons in Bose-Einstein condensates. *Phys. Rev. Lett.* **83,** 5198–5201 (1999).
9. Denschlag, J. *et al.* Generating solitons by phase engineering of a Bose-Einstein condensate. *Science* **287,** 97–100 (2000).
10. Anderson, B. P. *et al.* Watching dark solitons decay into vortex rings in a Bose-Einstein condensate. *Phys. Rev. Lett.* **86,** 2926–2929 (2001).
11. Pérez-García, V., Michinel, H. & Herrero, H. Bose-Einstein solitons in highly asymmetric traps. *Phys. Rev. A* **57,** 3837–3842 (1998).
12. Muryshev, A. E., van Linden van den Heuvell, H. B. & Shlyapnikov, G. V. Stability of standing matter waves in a trap. *Phys. Rev. A* **60,** R2665–R2668 (1999).
13. Carr, L. D., Leung, M. A. & Reinhardt, W. P. Dynamics of the Bose-Einstein condensate: quasi-one-dimension and beyond. *J. Phys. B* **33,** 3983–4001 (2000).
14. Kivshar, Y. S., Alexander, T. J. & Turitsyn, S. K. Nonlinear modes of a macroscopic quantum oscillator. *Phys. Lett. A* **278,** 225–230 (2001).
15. Schreck, F. *et al.* Quasipure Bose-Einstein condensate immersed in a Fermi sea. *Phys. Rev. Lett.* **87,** 080403-1–080403-4 (2001).
16. Görlitz, A. *et al.* Realization of Bose-Einstein condensates in lower dimensions. *Phys. Rev. Lett.* **87,** 130402-1–130402-4 (2001).
17. Truscott, A. G., Strecker, K. E., McAlexander, W. I., Partridge, G. B. & Hulet, R. G. Observation of Fermi pressure in a gas of trapped atoms. *Science* **291,** 2570–2572 (2001).
18. McAlexander, W. I. Collisional Interactions in an Ultracold Lithium Gas. Thesis, Rice Univ. (2000).
19. Tiesinga, E., Verhaar, B. J. & Stoof, H. T. C. Threshold and resonance phenomena in ultracold ground-state collisions. *Phys. Rev. A* **47,** 4114–4122 (1993).
20. Inouye, S. *et al.* Observation of Feshbach resonances in a Bose–Einstein condensate. *Nature* **392,** 151–154 (1998).
21. Roberts, J. L., Claussen, N. R., Cornish, S. L. & Wieman, C. E. Magnetic field dependence of ultracold collisions near a Feshbach resonance. *Phys. Rev. Lett.* **85,** 728–731 (2000).
22. Zakharov, V. E. & Shabat, A. B. Exact theory of two-dimensional self-focusing and one-dimensional self-modulation of waves in nonlinear media. *Sov. Phys. JETP* **34,** 62–65 (1972).
23. Carr, L. D., Clark, C. W. & Reinhardt, W. P. Stationary solutions of the one-dimensional nonlinear Schrödinger equation. II. Case of attractive nonlinearity. *Phys. Rev. A* **62,** 063611-1–063611-10 (2000).
24. Tai, K., Hasegawa, A. & Tomita, A. Observation of modulational instability in optical fibers. *Phys. Rev. Lett.* **56,** 135–138 (1986).
25. Gordon, J. P. Interaction forces among solitons in optical fibers. *Opt. Lett.* **8,** 596–598 (1983).
26. Hasegawa, A. *Optical Solitons in Fibers* (Springer, New York, 1990).
27. Lenz, G., Meystre, P. & Wright, E. M. Nonlinear atom optics. *Phys. Rev. Lett.* **71,** 3271–3274 (1993).
28. Kasevich, M. A. Atom interferometry with Bose-Einstein condensed atoms. *C.R. Acad. Sci. IV* **2,** 497–507 (2001).

**Acknowledgements**

We thank W. I. McAlexander for providing the coupled channels calculation, B. Luey for making the magnetic coils, and T. Killian and H. Stoof for discussions. This work was supported by the US National Science Foundation, NASA, the Office of Naval Research and the Welch Foundation.

**Competing interests statement**

The authors declare that they have no competing financial interests.

Correspondence and requests for materials should be addressed to R.G.H. (e-mail: randy@atomcool.rice.edu).

# Spin-galvanic effect

**S. D. Ganichev*†, E. L. Ivchenko†, V. V. Bel'kov†, S. A. Tarasenko†, M. Sollinger*, D. Weiss*, W. Wegscheider*‡ & W. Prettl***

** Fakultät für Physik, Universität Regensburg, D-93040 Regensburg, Germany*
*† A.F. Ioffe Physico-Technical Institute of the RAS, 194021 St Petersburg, Russia*
*‡ Walter Schottky Institut, TU München, 85748 Garching, Germany*

**There is much recent interest in exploiting the spin of conduction electrons in semiconductor heterostructures together with their charge to realize new device concepts[1]. Electrical currents are usually generated by electric or magnetic fields, or by gradients of, for example, carrier concentration or temperature. The electron spin in a spin-polarized electron gas can, in principle, also drive an electrical current, even at room temperature, if some general symmetry requirements are met. Here we demonstrate such a 'spin-galvanic' effect in semiconductor heterostructures, induced by a non-equilibrium, but uniform population of electron spins. The microscopic origin for this effect is that the two electronic sub-bands for spin-up and spin-down electrons are shifted in momentum space and, although the electron distribution in each sub-band is symmetric, there is an inherent asymmetry in the spin-flip scattering events between the two sub-bands. The resulting current flow has been detected by applying a magnetic field to rotate an optically oriented non-equilibrium spin polarization in the direction of the sample plane. In contrast to previous experiments, where spin-polarized currents were driven by electric fields in semiconductor[2,3], we have here the complementary situation where electron spins drive a current without the need of an external electric field.**

Although it is usually ignored, it is well known that the spin degeneracy of sub-bands in semiconductor quantum well (QW) structures can be lifted, owing to terms linear in the wavevector **k** resulting from the spin orbit interaction in asymmetric potentials[4,5]. For a two-dimensional electron gas (2DEG) system, this leads to the situation sketched in Fig. 1. The electron energy band splits into two sub-bands which are shifted in **k**-space and each of the bands comprise states with spin up or down. In this band structure spin polarization means that one sub-band is occupied up to higher energies than the other. This is depicted in Fig. 1, illustrating that there are more spin-down than spin-up electrons. Can such a situation of uniform spin polarization cause an electric current? As long as the carrier distribution in each sub-band is symmetric around the sub-band minimum at $k_{x_\pm}$ no current flows. However, asymmetric **k**-dependent spin relaxation events can occur, indicated

by the dashed arrows in Fig. 1, which result in a current flow. This means that a current is driven by a homogeneous spin polarization. Below we describe the observation of such a current.

Phenomenologically, an electric current can be linked by general symmetry arguments to the electron's averaged spin **S** by

$$j_\alpha = \sum_\gamma Q_{\alpha\gamma} S_\gamma \qquad (1)$$

where $j$ is an electric current density, $Q$ is a second-rank pseudo-tensor, and $\alpha, \gamma = 1, 2$ indicate coordinates. Non-vanishing tensor components $Q_{\alpha\gamma}$ can only exist in non-centrosymmetric systems belonging to one of the gyrotropic classes[6]. In zinc-blende-based heterojunctions with a 2DEG, non-zero components of $Q_{\alpha\gamma}$ exist in contrast to the corresponding bulk crystals[7]. In our (001)-grown heterojunctions with the $C_{2v}$ symmetry only two linearly independent components, $Q_{xy}$ and $Q_{yx}$, are different from zero ($x \| [1\bar{1}0]$ and $y \| [110]$) where $x$ and $y$ are cartesian coordinates. Hence, to observe a spin-polarization-driven current a spin component lying in the plane of the heterojunctions is required (for example, $S_y$ in Fig. 2).

To achieve an in-plane spin orientation in experiment one could either use spin selective contacts[8] (see Fig. 2a) or optical orientation[9] by using circularly polarized light. Although significant progress concerning electrical spin injecting has been made recently[10–12], reliable spin-injection into lateral low-dimensional electron systems—at room temperature—is still a challenge. Furthermore, electrical spin injection causes, apart from the driving current, a laterally inhomogeneous spin polarization and hence additional driving forces for current flow which would hamper the unambiguous demonstration of the effect described here. Instead, we use optical spin orientation, which ensures a homogeneous non-equilibrium spin polarization and directly proves the spin-galvanic effect. In this case of exciting electrons from the valence band to the conduction band the conduction band gets selectively spin-populated owing to selection rules which allow transitions by circularly polarized light only if the spin of the electron is changed by $\pm 1$. In addition to this method we have also used circularly polarized terahertz radiation causing intraband instead of interband excitation. One interesting aspect of employing terahertz radiation is that only one type of carriers, electrons or holes, is involved. In this respect, the effect of intraband spin orientation[13] is indeed very close to electrical spin injection.

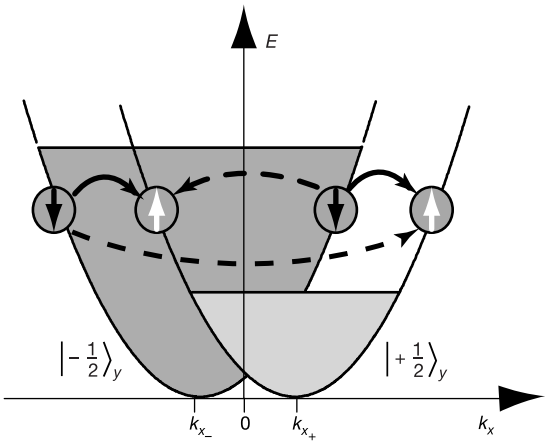


**Figure 1** Microscopic origin of the spin-galvanic current in the presence of **k**-linear terms in the electron hamiltonian. The $\sigma_y k_x$ term in the hamiltonian splits the conduction band into two parabolas with the spin $\pm 1/2$ in the $y$ direction. If one spin sub-band is preferentially occupied, for example, by spin injection (the $|-1/2\rangle_y$-states shown in the figure) asymmetric spin-flip scattering results in a current in the $x$ direction. The rate of spin-flip scattering depends on the value of the initial and final **k**-vectors. There are four distinct spin-flip scattering events possible, indicated by the arrows. The transitions sketched by dashed arrows yield an asymmetric occupation of both sub-bands and hence a current flow. If, instead of the spin-down sub-band, the spin-up sub-band is preferentially occupied the current direction is reversed.

It has been shown before that irradiation of quantum wells with circularly polarized light can result in a photocurrent caused by non-uniformly distributing photoexcited carriers in **k**-space according to optical selection rules and energy and momentum conservation. This is the circular photogalvanic effect observed recently in a 2DEG[14]. In order to achieve a uniform distribution in spin sub-bands and to exclude this circular photogalvanic effect we use the geometry depicted in Fig. 2b, where the photogalvanic current is identical to zero for normal incidence of the light[14]. In this geometry, optical excitation yields a steady-state spin orientation $S_{0z}$ in the $z$ direction with the generation rate $\dot{S}_z$ proportional to the intensity of the radiation. To obtain an in-plane component of the spins, necessary for the effect we describe here, a magnetic field, $B$, was applied (Fig. 2b). The field perpendicular to both the light-propagation direction $\hat{e}_z$ and the optically oriented spins rotates the spins into the plane of the 2DEG owing to Larmor precession. With the magnetic field oriented along the $x$ axis we obtain a non-equilibrium spin polarization $S_y$ which reads, after time averaging[7]:

$$S_y = -\frac{\omega_L \tau_{s\perp}}{1 + (\omega_L \tau_s)^2} S_{0z} \qquad (2)$$

where $\tau_s = \sqrt{\tau_{s\|}\tau_{s\perp}}$ and $\tau_{s\|}, \tau_{s\perp}$ are the longitudinal and transverse electron-spin-relaxation times, $\omega_L = g\mu_B B_x/\hbar$ is the Larmor frequency, $g$ is the in-plane effective electron $g$-factor, $\mu_B$ is the Bohr magneton, and $S_{0z} = \tau_{s\|}\dot{S}_z$ is the steady-state electron spin polarization in the absence of the magnetic field. Using the Larmor precession we prepared the situation sketched in Fig. 1 where the spin polarization $S_y$ lies in the plane. The denominator in equation (2) yielding the decay of $S_y$ for $\omega_L$ exceeding the inverse spin-relaxation time is well known from the Hanle effect[15].

The experiments were carried out at room temperature ($T = 293$ K) and at liquid helium temperature on $n$-GaAs/AlGaAs single quantum wells of 15-nm width and on GaAs single heterojunctions. The (001)-oriented samples grown by molecular beam epitaxy contain 2DEG systems with electron densities $n_s \simeq 2 \times 10^{11}\,\mathrm{cm}^{-2}$ and mobilities $\mu$ above $10^6\,\mathrm{cm}^2\,\mathrm{V}^{-1}\,\mathrm{s}^{-1}$ at $T = 4.2$ K. Two pairs of contacts were centred on opposite sample edges along the directions $x \| [1\bar{1}0]$ and $y \| [110]$ (see inset in Fig. 3). Complementary measurements were also carried out on $p$-GaAs multiple quantum-well structures containing 20 wells of 15-nm width with hole densities in each well $p_s = 2 \times 10^{11}\,\mathrm{cm}^{-2}$ and $\mu = 5 \times 10^5\,\mathrm{cm}^2\,\mathrm{V}^{-1}\,\mathrm{s}^{-1}$.

At room temperature a magnetic field of up to 1 T was generated by an electromagnet. For the low-temperature measurements the samples were placed in a cryostat with a split-coil superconducting magnet yielding a field $B$ of up to 3 T. For optical interband excitation a continuous-wave Ti:sapphire laser was used at a wavelength of $\lambda = 0.777\,\mu$m. In order to extract the spin-galvanic current the linearly polarized laser beam was transmitted through a

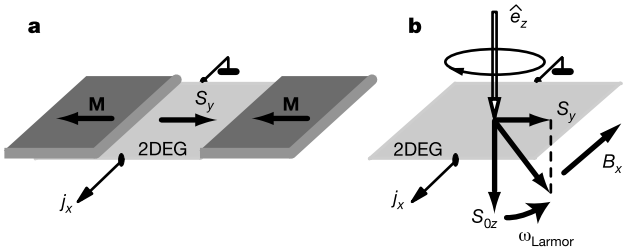


**Figure 2** Two ways of generating an in-plane spin-polarization. **a**, The spin injection from ferromagnetic contacts of magnetization **M** into the two-dimensional electron gas (2DEG). **b**, The optical orientation in combination with an in-plane magnetic field $B_x$. Spins, initially aligned along the $z$ direction are rotated into the $y$ direction by $B_x$.

photoelastic modulator which yields a periodically oscillating polarization between right-circular and left-circular. The current was recorded by a lock-in amplifier in phase with the modulator. For intraband excitation we used the $\lambda = 148\,\mu$m line of a pulsed ammonia laser[16]. The current of unbiased samples was measured by the voltage drop on a 50 Ω load resistor in a closed circuit configuration.

Both for visible and terahertz radiation a current has been observed for all *n*-type samples after applying an in-plane magnetic field (Figs 3 and 4). For small magnetic fields $B$ where $\omega_L\tau_s < 1$ holds, the spin-galvanic current increases linearly as expected from equations (1) and (2). This is seen in the room-temperature data of Fig. 3 and in the 4.2 K data in Fig. 4 for $B \leq 1$ T. The polarity of the current depends on the direction of the excited spins ($\pm z$-direction for right- or left-circularly polarized light, respectively) and on the direction of the applied magnetic field ($\pm x$ direction). The current is parallel (or anti-parallel) to the magnetic field vector. Comparing the power sensitivity for visible and terahertz excitation we find them to be of the same order of magnitude as seen in Fig. 3. However, we note that the current contribution per photon is larger by two orders of magnitude for interband excitation. This is due to a more effective spin generation rate by interband excitation. It may even be larger, because the signal gets partially shortened by photogenerated carriers in the semi-insulating substrate.

For higher magnetic fields the current saturates and decreases upon further increase of $B$, as shown in Fig. 4. This is ascribed to the Hanle effect, see equation (2). The observation of the Hanle effect demonstrates that free carrier intraband transitions can polarize the spins of electron systems. The measurements allow us to obtain the spin-relaxation time $\tau_s$ from the peak position of the photocurrent where $\omega_L\tau_s = 1$ holds if the $g$-factor is known. The $g$-factor of quantum wells, however, depends strongly on structural details. This leads to an uncertainty in the measured spin lifetime itself. Using the theoretically estimated[17] value of $g = -0.2$ results in $\tau_s = 40$ ps at 4.2 K. Spin-relaxation times of the same order of magnitude as derived here have been obtained by photoluminescence measurements[18]. However, direct comparison of these results with our data is difficult, because optical recombination does not detect the spin-relaxation time at the Fermi energy of the 2DEG, as in the present case of monopolar spin orientation. Published data on Faraday rotation experiments, which give access to spin relaxation at the Fermi level, however, refer to materials which are not directly comparable to our samples[19,20].

Because the in-plane $g$-factor for heavy holes is very small[21], the associated spin-galvanic effect is expected to be negligible. Indeed no magnetic-field-induced current has been observed in *p*-GaAs quantum wells at terahertz excitation causing spin polarization of holes only. We note that a magnetic-field-induced circular photogalvanic effect in *p*-type bulk materials was previously observed in GaAs at intraband excitation[22]. However, this effect is not due to spin orientation and does not occur in *p*-type quantum wells owing to spatial quantization[23]. Only for visible excitation, which polarizes both electrons and holes, has a current signal been detected in *p*-type samples (see Fig. 3). This current is due to the spin polarization of electrons again, which are in this case the minority carriers generated by interband excitation.

Microscopically, the spin-galvanic effect is caused by the asymmetric spin-flip relaxation of spin-polarized electrons in systems with **k**-linear contributions to the effective hamiltonian. The lifting of spin degeneracy of 2DEG depicted in Fig. 1 is a consequence of a contribution to the hamiltonian of the form $\hat{H}_{\mathbf{k}} = \sum_{\gamma\alpha}\beta_{\alpha\gamma}\sigma_\alpha k_\gamma$ where $\sigma_\alpha$ are the Pauli spin matrices and $\beta_{\alpha\gamma}$ is a pseudo-tensor subjected to the same symmetry restriction as the pseudo-tensor $Q_{\alpha\gamma}$ used in equation (1). Figure 1 sketches the electron energy spectrum with the $\beta_{yx}\sigma_y k_x$ term included. Spin orientation in the $y$ direction causes an unbalanced population in the spin-down and spin-up sub-bands. The current flow is caused by the **k**-dependent spin-flip relaxation processes. Spins oriented in the $y$ direction are scattered along $k_x$ from the higher filled (for example, spin-down) sub-band, $|-1/2\rangle_y$, to the less filled spin-up sub-band, $|+1/2\rangle_y$. Four quantitatively different spin-flip scattering events exist and are sketched in Fig. 1 by bent arrows. The spin-flip scattering rate depends on the values of the wavevectors of the initial and the final states, respectively[24]. Therefore spin-flip transitions, shown by solid arrows in Fig. 4, have the same rates. They preserve the symmetric distribution of carriers in the sub-bands and, thus, do not yield a current. However, the two scattering processes shown by broken arrows are not equivalent and generate an asymmetric carrier distribution around the sub-band minima in both sub-bands. This asymmetric distribution results in a current flow along the $x$ direction. Within our model of elastic scattering the current is not

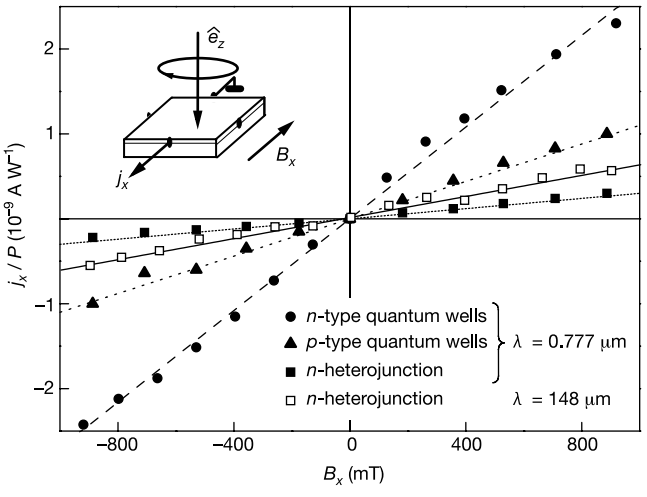


**Figure 3** Current density $j_x$ normalized to the radiation power $P$ as a function of the magnetic field $B$ for normally incident circularly polarized radiation at room temperature for various samples and wavelengths. Filled symbols: $\lambda = 0.777\,\mu$m, $P = 100$ mW. Triangles, squares and circles correspond to *n*-type and *p*-type multiple quantum wells, and an *n*-type GaAs/AlGaAs heterojunction, respectively. Open squares: *n*-type GaAs/AlGaAs heterojunction, $\lambda = 148\,\mu$m, $P = 20$ kW. The inset shows the geometry of the experiment where $\hat{e_z}$ indicates the direction of the incoming light.

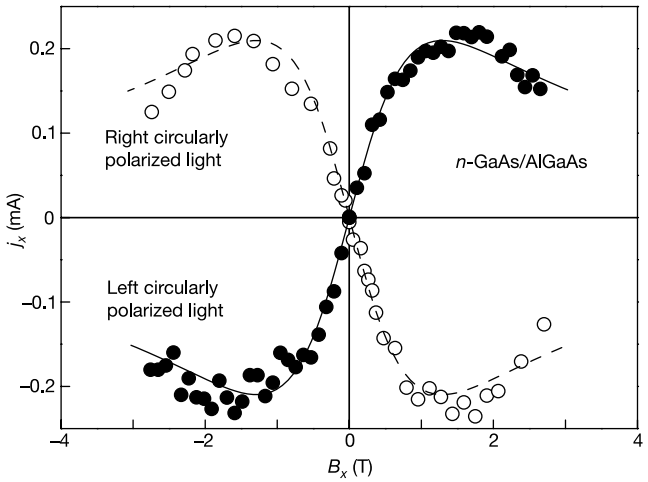


**Figure 4** Current $j_x$ as a function of magnetic field $B$ for normally incident right-handed (open circles) and left-handed (filled circles) circularly polarized radiation at $\lambda = 148\,\mu$m and radiation power 20 kW. Measurements are presented for a *n*-GaAs/AlGaAs single heterojunction at $T = 4.2$ K. Curves are fitted from equation (2) using the same value of the spin relaxation time $\tau_s$ and scaling of the $j_x$ value for the solid curve as for the dashed curve.

spin-polarized because the same number of spin-up and spin-down electrons move in the same direction with the same velocity. In the case of inelastic scattering the current may be polarized.

The uniformity of the spin polarization in space is preserved during the scattering processes. Therefore, the spin-galvanic effect differs from surface currents induced by inhomogeneous spin orientation[25]. It also differs from other experiments where the spin current is caused by gradients of potentials, concentrations and so on, like the spin-voltaic effect[26,27] and the photo-voltaic effect, which occur in inhomogeneous samples, and like the 'para-magnetic metal-ferromagnet' junction or *p-n* junctions. When considering spintronic devices involving heterojunctions, spin-galvanic current must be taken into account. □

Received 3 January; accepted 25 March 2002.


1. Wolf, S. A. *et al.* Spintronics: a spin-based electronics vision for the future. *Science* **294,** 1488–1495 (2001).
2. Hägele, D. *et al.* Spin transport in GaAs. *Appl. Phys. Lett.* **73,** 1580–1582 (1998).
3. Kikkawa, J. M. & Awschalom, D. D. Lateral drag of spin coherence in gallium arsenide. *Nature* **397,** 139–141 (1999).
4. Bychkov, Y. A. & Rashba, E. I. Properties of a 2D electron gas with lifted spectral degeneracy. *Sov. JETP Lett.* **39,** 78–81 (1984).
5. D'yakonov, M. I. & Kocharovskii, V. Yu. Spin relaxation of two-dimensional electrons in noncentrosymmetric semiconductors. *Sov. Phys. Semicond.* **20,** 110–111 (1986).
6. Koopmans, B., Santos, P. V. & Cardona, M. Optical activity in seminconductors: stress and confinement effects. *Phys. Status Solidi* **205,** 419–463 (1998).
7. Ivchenko, E. L., Lyanda-Geller, Yu, B. & Pikus, G. E. Current of thermalized spin-oriented photocarriers. *Sov. Phys. JETP* **71,** 550–557 (1990).
8. Fiederling, R. *et al.* Injection and detection of spin-polarized current in a light-emitting diode. *Nature* **402,** 787–789 (1999).
9. Meier, F. & Zakharchenya, B. P. (eds) *Optical Orientation* 1–523 (Elsevier Science, Amsterdam, 1984).
10. Hammar, P. R. & Johnson, M. Spin-dependent current transmission across a ferromagnet-insulator-two-dimensional electron gas junction. *Appl. Phys. Lett.* **79,** 2591–2593 (2001).
11. Zhu, H. J. *et al.* Room-temperature spin injection from Fe into GaAs. *Phys. Rev. Lett.* **87,** 016601-1–016601-4 (2001).
12. Hanbicki, A. T. *et al.* Efficient electrical spin injection from a magnetic metal/tunnel barrier contact into a semiconductor. *Appl. Phys. Lett.* **80,** 1240–1242 (2002).
13. Tarasenko, S. A. & Ivchenko, E. L. Spin orientation of two-dimensional electron gas under intraband optical pumping. Preprint cond-mat/0202471 at ⟨http://xxx.lanl.gov⟩ (2002).
14. Ganichev, S. D. *et al.* Conversion of spin into direct electric current in quantum wells. *Phys. Rev. Lett.* **86,** 4358–4361 (2001).
15. Hanle, W. Über magnetische Beeinflussung der Polarisation der Resonanzfluoreszenz. *Z. Phys.* **30,** 93–105 (1924).
16. Ganichev, S. D. Tunnel ionization of deep impurities in semiconductors induced by terahertz electric fields. *Physica B* **273–274,** 737–742 (1999).
17. Ivchenko, E. L., Kiselev, A. A. & Willander, M. Electronic *g*-factor in biased quantum wells. *Solid State Commun.* **102,** 375–378 (1997).
18. Damen, T. C. *et al.* Subpicosecond spin relaxation dynamics of excitons and free carriers in GaAs quantum wells. *Phys. Rev. Lett.* **67,** 3432–3435 (1991).
19. Kikkawa, J. M. *et al.* Room-temperature spin memory in two-dimensional electron gases. *Science* **277,** 1284–1287 (1997).
20. Sandu, J. S. *et al.* Gateable suppression of spin relaxation in semiconductors. *Phys. Rev. Lett.* **86,** 2150–2153 (2001).
21. Marie, X. *et al.* Hole spin quantum beats in quantum-well structures. *Phys. Rev. Lett.* **60,** 5811–5817 (1999).
22. Andrianov, A. V. & Yaroshetskii, I. D. Magnetic-field-induced circular photovoltaic effect in semiconductors. *Sov. JETP Lett.* **40,** 882–884 (1984).
23. Ivchenko, E. L., Lyanda-Geller, Yu, B. & Pikus, G. E. Circular magnetophotocurrent and spin splitting of band states in optically-inactive crystals. *Solid State Commun.* **69,** 663–665 (1989).
24. Averkiev, N. S., Golub, L. E. & Willander, M. Spin relaxation anisotropy in two-dimensional semiconductor systems. Preprint cond-mat/0202437 at ⟨http://xxx.lanl.gov⟩ (2002).
25. Averkiev, N. S. & D'yakonov, M. I. Current due to inhomogeneity of the spin orientation of electrons in a semiconductor. *Sov. Phys. Semicond.* **17,** 393–395 (1983).
26. Johnson, M. & Silsbee, R. H. Interfacial charge-spin coupling: injection and detection of spin magnetization in metals. *Phys. Rev. Lett.* **55,** 1790–1793 (1985).
27. Zutic, I., Fabian, J. & Das Sarma, S. Spin-polarized transport in inhomogeneous magnetic semiconductors: theory of magnetic/nonmagnetic *p–n* junctions. *Phys. Rev. Lett.* **88,** 066603-1–066603-4 (2001).



### Acknowledgements

We thank D. I. Kovalev, W. Schoepe and M. Bichler for helpful discussions and support. We acknowledge financial support from the DFG, the RFFI and INTAS.


### Competing interests statement

The authors declare that they have no competing financial interests.

Correspondence and requests for materials should be addressed to S.D.G. (e-mail: sergey.ganichev@physik.uni-regensburg.de).

# Terahertz semiconductor-heterostructure laser

**Rüdeger Köhler*, Alessandro Tredicucci*, Fabio Beltram*, Harvey E. Beere†, Edmund H. Linfield†, A. Giles Davies†, David A. Ritchie†, Rita C. Iotti‡ & Fausto Rossi‡**

** NEST-INFM and Scuola Normale Superiore, Piazza dei Cavalieri 7, 56126 Pisa, Italy*

*† Cavendish Laboratory, University of Cambridge, Madingley Road, Cambridge CB3 0HE, UK*

*‡ INFM and Dipartimento di Fisica, Politecnico di Torino, Corso Duca degli Abruzzi 24, 10129 Torino, Italy*

**Semiconductor devices have become indispensable for generating electromagnetic radiation in everyday applications. Visible and infrared diode lasers are at the core of information technology, and at the other end of the spectrum, microwave and radio-frequency emitters enable wireless communications. But the terahertz region (1–10 THz; 1 THz = $10^{12}$ Hz) between these ranges has remained largely underdeveloped, despite the identification of various possible applications—for example, chemical detection, astronomy and medical imaging[1–4]. Progress in this area has been hampered by the lack of compact, low-consumption, solid-state terahertz sources[5–9]. Here we report a monolithic terahertz injection laser that is based on interminiband transitions in the conduction band of a semiconductor (GaAs/AlGaAs) heterostructure. The prototype demonstrated emits a single mode at 4.4 THz, and already shows high output powers of more than 2 mW with low threshold current densities of about a few hundred A cm$^{-2}$ up to 50 K. These results are very promising for extending the present laser concept to continuous-wave and high-temperature operation, which would lead to implementation in practical photonic systems.**

In conventional semiconductor lasers, light is generated by the radiative recombination of conduction band electrons with valence band holes across the bandgap of the active material; in contrast, electrons in a quantum-cascade laser propagate through a potential staircase of coupled quantum wells, where the conduction band is split by quantum confinement into a number of distinct sub-bands[10]. By choice of layer thickness and applied electric field, lifetimes and tunnelling probabilities of each level are engineered in order to obtain population inversion between two sub-bands in a series of identical repeat units. Injector/collector structures connect these active regions, allowing electrical transport through injection of carriers into the upper laser level, and extraction of carriers from the lower laser level. The radiation frequency is determined by the energy spacing of the lasing sub-bands, allowing in principle operation at arbitrarily long wavelengths. The quantum-cascade scheme has thus long been the preferred choice in many attempts to fabricate a terahertz semiconductor laser. Although electroluminescent devices have been reported by several groups[11–14], laser action has been shown only at much shorter wavelengths[15,16]. In fact, above the forbidden phonon band of the material, direct electron–longitudinal optical (LO) phonon scattering processes can be conveniently used to achieve large population inversions[16]. Furthermore, an additional problematic issue for the terahertz range stems from the fact that conventional laser waveguides are not suitable, owing to large free-carrier absorption losses and practical limitations on the thickness of epilayer growth.

As in all lasers, efficient depletion of the lower level is essential, and long lifetimes of the upper level are highly desirable. Up until now, proposed terahertz quantum-cascade designs focused mainly on the latter aspect. To this end, structures have featured narrow injector minibands to both suppress scattering of electrons from the